Journal of The Electrochemical Society, **153** (3) A527-A532 (2006)
0013-4651/2006/153(3)/A527/6/$20.00 © The Electrochemical Society

Organic Photovoltaics Interdigitated on the Molecular Scale

Alex B. F. Martinson, Aaron M. Massari,* Suk Joong Lee, Richard W. Gurney, Kathryn E. Splan, Joseph T. Hupp, and SonBinh T. Nguyen**

Department of Chemistry, Northwestern University, Evanston, Illinois 60208, USA

Phosphonated porphyrin frameworks that are porous to an electron-accepting perylenediimide are systematically interdigitated with a phosphonated form of the diimide to form bulk heterojunctions. When employed in photovoltaics, these molecularly interlaced heterojunctions provide large junction areas while retaining the phase connectivity of traditional bilayer heterojunctions. Zirconium phosphonate linkages facilitate layer-by-layer chromophore assembly from solution under ambient conditions. The dependence of photovoltaic performance on heterojunction architecture is investigated.
 [DOI: 10.1149/1.2165788]

Manuscript submitted September 21, 2005; revised manuscript received December 7, 2005.
Available electronically January 25, 2006.

Efficient conversion of solar radiation into electricity is a compelling scientific and economic goal. While predominately organic devices are currently not as efficient as inorganic photovoltaics (PVs), their efficiencies have been steadily increasing over the past decade. The most significant advances are attributable to greater control over the donor-acceptor interface where photogenerated excitons are dissociated into electrons and holes.[1-3]

The incident-photon-to-current-efficiency (IPCE) of an organic photovoltaic is a product of the light harvesting efficiency (LHE), exciton diffusion/dissociation efficiency (η_{ED}), and charge carrier collection efficiency (η_{CC}). Careful selection of chromophores that absorb a broad range of the solar spectrum with large extinction ensures ample absorption with minimal thickness. Yet, for the best chromophores to date, the optical absorption length is significantly larger than the exciton diffusion distance.[4,5] Thus, η_{ED} is low in bilayer cells thick enough to provide sufficient LHE. Lacking a proximal heterojunction (at which charge separation can occur), the majority of excitons formed will radiatively or thermally decay before reaching the heterojunction (Fig. 1a). This problem has been circumvented by "blending" the donor and acceptor layers to decrease the distance excitons are required to travel to reach the heterojunction. Most notably, polymers and fullerene derivatives have been blended to produce devices that are up to 3.5% power efficient.[2] Thin films derived from small organic molecules have also been blended from their respective donor and acceptor components by either annealing or self-assembly.[5,6] In such heterojunctions, often referred to as bulk heterojunctions, η_{ED} is highly dependent on the degree to which the donor and acceptor are interlaced. In a blended heterojunction cell, η_{ED} can be near unity as confirmed by essentially complete quenching of photoluminescence.[7] While bulk heterojuctions produced by blending have shown good LHE and η_{ED}, modest IPCEs suggest that η_{CC} limits device efficiency. Poor charge collection may result from several factors including low carrier mobilities and a tortuous or discontinuous path for charge carriers through the photoactive phases. Figure 1b illustrates the isolated heterojunction areas that may form upon blending. When a distance-efficient, energetically facile path through which the charge may migrate is absent, charge carriers will tend to recombine rather than exit the photocell as measurable current.

We hypothesized that by shrinking the heterojunction dimensions to the molecular scale such that every donor is in contact with acceptor molecules (and vice versa), the issue of exciton diffusion could be fully mitigated. This is reminiscent of the use of covalently linked porphyrin/fullerene dyads in organic photovoltaic cells.[8] We further reasoned that if molecular donors and acceptors each could be organized in aligned fashion, short charge transport distances could be obtained, potentially decreasing charge recombination. Additionally, formation of isolated heterojunctions could likely be avoided. As described below, we have used a layer-by-layer zirconium phosphonate (ZrP) assembly approach to obtain porous aligned donor structures that are then in-filled with similarly aligned acceptor structures. We find interdigitated donor/acceptor structures to be superior to bilayer structures of the same materials when used as photovoltaic components. They are also superior to composition-randomized donor/acceptor structures. Nevertheless, the absolute IPCEs of the interdigitated structures are still low, pointing to the importance of additional design considerations, especially for optimization of carrier collection efficiency.

Experimental

Materials.— Acetonitrile (ACN) and dimethylsulfoxide (DMSO) were purified using the Dow-Grubbs solvent system[9] installed by Glass Contours, Inc. (Laguna Beach, CA). Concentrated HCl, concentrated H_2SO_4, concentrated HNO_3, 30% hydrogen peroxide, and hexanes were obtained from Fischer Scientific and used as received. Electrochemical grade potassium nitrate (KNO_3) was obtained from Fluka. All other reagents were obtained from Aldrich and used as received. Single-sided indium tin oxide (ITO)-coated unpolished float glass slides (ITO thickness = 120–160 nm, R_s = 8–12 Ω) were obtained from Delta Technologies, Ltd. [Water was purified and deionized (18 MΩ cm resistivity) by using a Millipore filtration and ion-exchange system.] Molecular square **1** and monomeric porphyrin **2** were synthesized as previously described.[10,11] Molecular modeling was carried out using HyperChem (version 6.0).

Synthesis of diphosphonated perylenediimide **3**.— Compound **3** was synthesized via a modification of a literature procedure.[12] In a 25-mL round-bottom flask, 3,4,9,10-perylenetetracarboxylic dianhydride (96.2 mg, 0.245 mol) and 3-aminopropylphosphonic acid (98 mg, 0.704 mol) were combined with imidazole (1 g). The resulting mixture was heated neat in an oil bath to approximately 100°C for 4 h, and then allowed to cool to room temperature. The crude reaction mixture was then dissolved in water and tetrahydrofuran (THF) was slowly added to precipitate the desired product. The resulting mixture was filtered over a glass frit; the solid precipitate was rinsed with THF and dried under vacuum overnight to yield pure **3** as a dark purple solid (116 mg, 75% yield). See Scheme 1.

Substrate preparation.— ITO substrates were cut into 4×0.9 cm pieces and degreased by soaking in acetone and rinsing with water. An ITO etching solution was prepared by adding concentrated HCl (5 mL), concentrated HNO_3 (1.25 mL), and concentrated Alconox solution (5 drops) to water (10 mL). This solution was then diluted to 25 mL with additional water, poured into a 30-mL vial, and heated to 80°C while stirring. An approximately 1-cm section of each substrate was soaked in the etching solution for 10 min to remove all the ITO, as verified by a subsequent test for conductivity. A well-defined etch may only be achieved by filling the etching solution to the top of the vial where etching vapors may be removed by the air flow of the hood. Removal of the ITO in this manner affords a suitable location for contacting the dark electrode

* Electrochemical Society Student Member.
** Electrochemical Society Active Member.

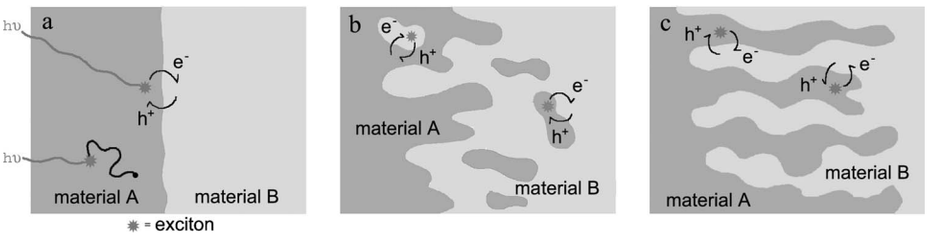

Figure 1. Idealized representation of **(a)** bilayer; **(b)** blended; and **(c)** interdigitated heterojunctions. Material A is taken to be the electron donor and material B the electron acceptor.

without risk of contacting the ITO, thus reducing the risk of short-circuiting the cell. The samples were then soaked in a 2:1 H_2SO_4:H_2O_2 mixture in a cold water bath for 15 min. (*Caution, mixture reacts violently with organics*.) The samples were then rinsed with water and dried in an 80°C oven for at least 15 min. The thus-hydroxylated substrates were then soaked in an anhydrous octanol solution of (3-aminopropyl)trimethoxysilane (55 mM) at 80°C for 15 min, yielding an amine-terminated surface. After rinsing with hexanes and water the samples were again dried at 80°C for at least 30 min. Phosphorylation of the surfaces was achieved by soaking in a dry acetonitrile solution of $POCl_3$ (10 mM) and 2,4,5-collidine (10 mM) for 20 min at room temperature. The phosphorylated substrates were then rinsed with ACN and water before being submerged in an aqueous $ZrOCl_2$ solution (25 mM) for at least 4 h to complete the zirconation step. Finally, samples were rinsed with water and dried under a stream of nitrogen before being stored under ambient conditions.

Multilayers of **1** and **2** were grown using well-established layer-by-layer deposition techniques with aqueous Zr^{4+}, as reported previously.[13-15] Substrates were consecutively soaked in an aqueous $ZrOCl_2$ solution (25 mM) for 30 min followed by a solution of **1** or **2** (0.02 mM) in dry DMSO for at least 3 h. Subsequent soaking of the samples for 10 min in DMSO and water, and rinsing them with fresh DMSO or water after each soak, ensures only ZrP-bound chromophores remain before growing the next layer. Because each chromophore has phosphonic acid functionalities on both ends, the cycle may be repeated indefinitely. Care was taken to minimize sample exposure to light by storing solutions and rinses in a dark box as well as performing growth under dark cover. Solutions of **1** and **2** in DMSO are sensitive to moisture and therefore were kept in a dark vacuum desiccator.

Layers of **3** were grown in a similar manner as those of **1** and **2** by alternately soaking the electrodes in an aqueous $ZrOCl_2$ solution (25 mM) for 30 min followed by exposure to an aqueous solution of **3** (0.2 mM) for 30 min. After successful ZrP growth of **3**, the substrates were soaked in water for 15 min. Deposition times were optimized to yield maximum absorbance per layer in a minimum amount of time. Film growth was monitored by UV-Vis-NIR spectroscopy using a Varian Cary 5000 spectrophotometer. Film thickness was determined via atomic-force microscopy (AFM) performed with a Digital Instruments Bioscope and a Nanoscope III controller in contact mode. To achieve an imageable step between the film and the bare surface, the glass side of a ZrP-assembled sample was deliberately scratched with a razor blade and rinsed vigorously with water to remove debris.[16] The AFM tip was positioned at the scratched region by using an inverted optical microscope (Nikon Eclipse TE300).

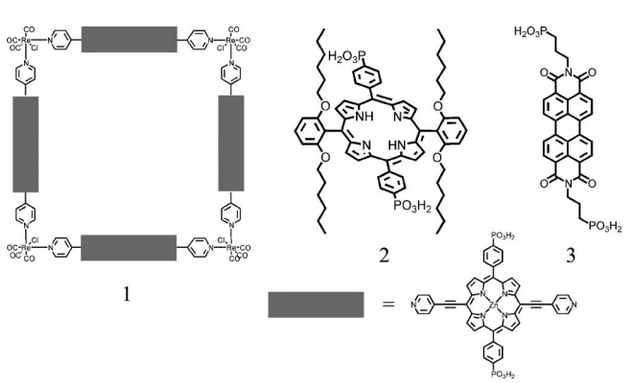

Scheme 1.

The dark electrode was deposited on the ITO side of the substrate by thermal evaporation of aluminum at 2.0×10^{-5} Torr at a rate of 0.1 nm/s. Approximately 60 nm of the metal was deposited as measured by an Inficon quartz crystal microbalance. Masking the top 1 cm and 1 mm along each long edge of the substrate with cellophane tape affords adequate space for independent contact to the Al and ITO.

Electrochemical measurements.— Electrochemical measurements of the thin films of **3** within porous frameworks of **1** and **2** were taken in aqueous KNO_3 electrolyte (0.1 M) using a three-electrode cell configuration (Pt wire counter electrode) on a CH Instruments 1202 potentiostat. All other electrochemical measurements of thin films were taken in tetrabutylammonium hexafluorophosphate electrolyte (0.1 M in anhydrous ACN) using a three-electrode cell configuration (Pt wire counter electrode) on a CH Instruments 900 potentiostat. Potentials were recorded vs a pseudo-Ag/AgCl reference electrode, but are reported vs ferrocenium/ferrocene as measured in situ.

Spectral and photochemical measurements.— Steady-state photoluminescence measurements were performed on a Jobin Yvon SPEX Fluorolog-3 spectrofluorimeter. Photovoltaic cells where illuminated using a 450-W Xe arc lamp and the excitation monochromator of a Jobin Yvon SPEX Fluorolog-3 spectrofluorimeter. Samples were illuminated through a 0.150 cm^2 hole. The illuminated area visible light (400 to 700 nm) flux was 147 mW/cm^2. Photocurrent and photovoltage measurements were acquired on a CH Instruments 1202 potentiostat using a two-electrode configuration with the reference and counter electrode tied together.

IPCEs were calculated according to the equation

$$\text{IPCE} = 1240 \times \text{photocurrent(uA cm}^{-2})/[\text{wavelength(nm)} \times \text{photon flux(uW cm}^{-2})]$$

The LHE was calculated assuming the measured absorbance is twice the actual 10-layer absorbance (due to simultaneous film growth on the insulating side of the ITO electrode), but the absorbance of completed devices is subsequently doubled assuming perfect reflectivity from the aluminum contact. The filter effect owing to growth on the insulating side of the ITO is included in IPCE calculations by applying an attenuating factor to the incident light intensity as a function of wavelength.

Results and Discussion

Zirconium phosphonate (ZrP) film growth.— Scheme 2 summarizes the approach used. (For simplicity of illustration, the superstructures shown are idealized as single-column stacks of squares having strictly vertical walls.) Advantage was taken of the known high affinity of Zr(IV) for phosphonates to generate robust thin films in layer-by-layer fashion.[14,15,17,18] Because each growth cycle entails two steps, only one monolayer of metal phosphonate is added per

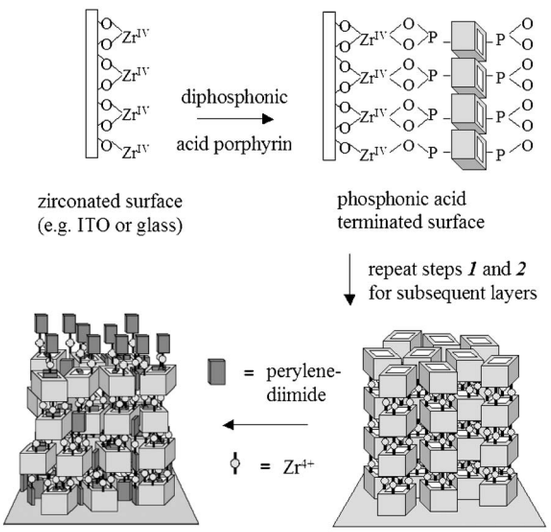

Scheme 2. Stepwise assembly of interlaced films porphyrin square **1** and perylene diimide **2**. For simplicity of illustration, the porphyrinic superstructure is idealized as single-column stacks of squares having strictly vertical walls.

cycle. Thus, the ZrP approach is particularly effective for growing films of precisely controlled thickness and, therefore, absorptivity.

Each cycle of film growth of the macromolecular porphyrin square **1** on indium-tin oxide consistently results in a 0.020 increase in the per-side normalized Soret band absorbance (Fig. 2a inset) and adds about 2 nm to the single-sided film thickness.[16] Identical assembly schemes using the diphosphonic acid porphyrin.[11] **2** and diphosphonic acid perylenediimide **3**, respectively, yield increases in Soret absorbance maximum of 0.030 and 0.007 per assembly cycle (Fig. 2b and c insets). Shown in the main panels of Fig. 2 are electronic absorption spectra for 10-layer films of each of the three chromophores. The most intense visible-region electronic transitions for **2** and **3** (but not **1**) are characterized by transition dipole moments oriented along the phosphonate functionalization axis, implying that film-based absorption may be polarized. Measurements of this kind with film of **2** and **3** indeed reveal polarization and establish that net orientation of both chromophores in the direction normal to the surface is attained.

The strategy for forming interdigitated thin-film structures relies upon first assembling a single-component film that is intrinsically porous on roughly the nanometer scale. This film is then back-filled with the second component. Previous electrochemical studies of the porosity of thin films of **1** (hollow molecular squares) revealed that they are permeable to redox probes having diameters less than 13 Å.[16] Similarly, films of **2** on ITO block probes greater than 14 Å in diameter but are permeable to smaller species. The porosity here is a consequence of the presence of bulky phenyl-ether substituents oriented perpendicular to the porphyrin plane.[11] The perpendicular configuration effectively prevents channel-blocking aggregation in the thin-film environment. As noted previously,[11] the sharp Soret band and increased fluorescence emission yield of films of **2** relative to less hindered porphyrin films provide strong supporting evidence for the inhibition of aggregation. Given that the modeled width of **3** is 6.6 Å, we expected it to readily infiltrate multilayer frameworks of **1** and **2**. Thus, iterative exposure of completed films of **1** or **2** to Zr^{4+} and **3** should grow the acceptor material as strands both within and upon the porphyrin frameworks (Scheme 2).

According to this growth scheme, the amount of **3** that is electrochemically addressable via the ITO electrode should systematically increase with the number of deposition cycles. At the same time, electrochemically inaccessible **3** should be deposited atop the

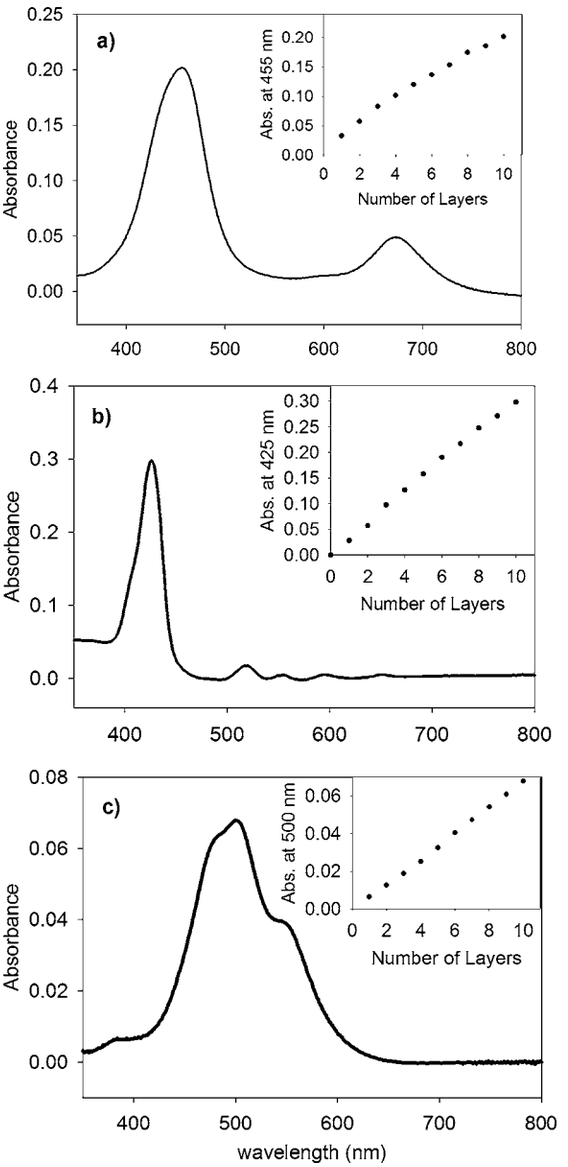

Figure 2. Absorption spectra of 10 layers of (a) **1**; (b) **2**, and (c) **3** on functionalized ITO corrected for absorption on the glass side. Insets: Absorption maxima as a function of the number of multilayers.

porphyrinic film. When diimide material grown within the porphyrin framework extends up sufficiently from the ITO surface to meet the ZrP diimide material grown upon the framework, redox mediation becomes possible and a substantial increase in the amount of electrochemically accessible diimide should be observed. Figure 3 shows the result of experiments in which successive layers of **3** are grown within and upon 10-layer films of **1** or **2**. The charge associated with voltammetric reduction of **3** gradually increases as additional growth cycles are completed. Between 6 and 8 cycles, however, the measured charge shows a substantially larger increase. We interpret this as a measure of the point at which the layers of **3** grown from the ITO surface establish redox contact with the layers of **3** grown atop the porphyrin films.

While it is clear from these experiments that **3** permeates both **1** and **2** to form heterojunctions, we were surprised that inner-layer/outer-layer redox communication could be achieved with less than 10 assembly cycles, since 10 layers of porphyrin material were used in each case. Atomic force microscopy measurements of intention-

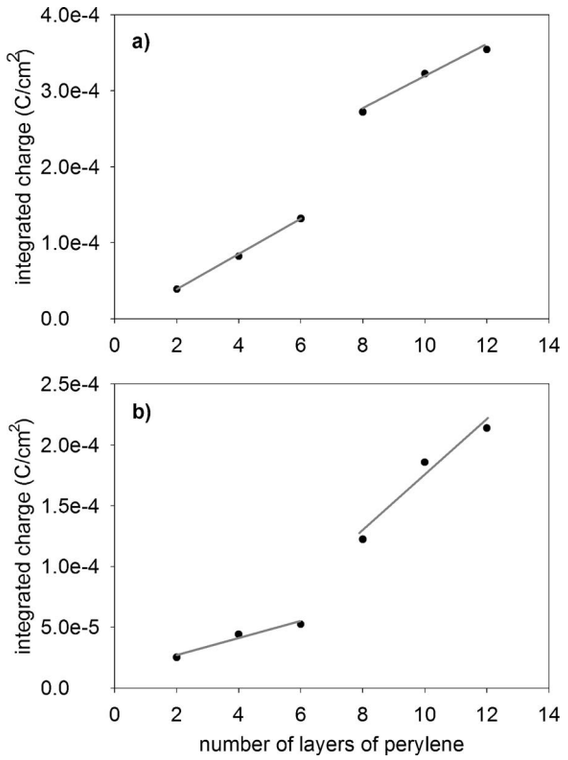

Figure 3. Plots of the integrated charge associated with the reduction of **3** within porphyrin frameworks: (a) **1**; and (b) **2**.

ally scratched films of **3** revealed an average "layer" thickness of about 3.8 nm, which exceeds the thickness of porphyrinic layers as well as the length of a fully extended molecule of **3**. Absorption spectra for **3**, both in solution and in films, are substantially broader than expected, indicating its aggregation in both environments. The layer thickness, then, corresponds to the length of an aggregate of **3**, rather than an isolated molecule of **3**.

Energetics of exciton dissociation.— To establish both the thermodynamic feasibility and the anticipated direction of excitonic dissociation, the relative energy levels of all participating species must be determined. Cyclic voltammetry (not shown) reveals an irreversible oxidation between +0.7 and +0.8 V vs ferrocene/ferrocenium for films of **1** on ITO. Determination of the ground-state/photoexcited-state energy gap was not possible for films of **1** due to their lack of fluorescence. Instead, an energy gap of 1.85 eV was established from the fluorescence spectrum of **1** in DMSO. Films of **2** irreversibly oxidize near 0.5 V and show an energy gap of 1.95 eV by fluorescence. Cyclic voltammetry on films of **3** reveals an irreversible oxidation at ~1.0 V and reductions at −0.95 and −1.22 V. A summary of energy levels is shown as Fig. 4, where the values are only estimates, given the irreversibility of the oxidation reactions. Additionally, the removal of solvent from the films upon photocell formation may alter the energy levels.

Film luminescence.— The degree to which excitons are quenched by these heterojunctions may be probed by examining thin-film photoluminescence. While films of **1** show insignificant emission, the nonaggregating nature of **2** leads to readily observable film emission with a maximum near 655 nm. When multilayers of **3** are interdigitated the emission from the selective excitation of **2** is quenched by up to 70%.

For comparison, two other chromophore/quencher geometries were examined, as sketched qualitatively in Fig. 5. In one, which we will designate **b**, the growth order of **2** and **3** was reversed. Because

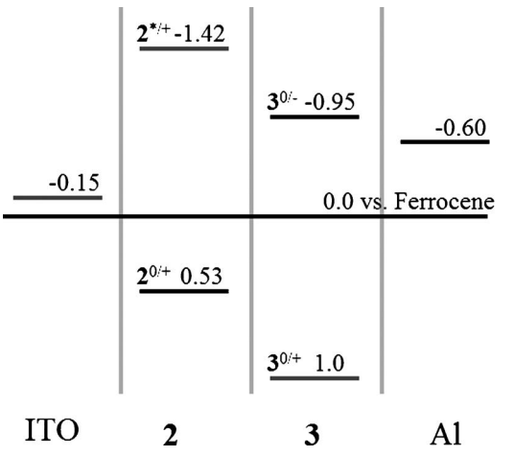

Figure 4. Approximate energy diagram for photovoltaic cell components. Both ground- and excited-state redox potentials are shown for **2** and **3**. The approximate potentials for $\mathbf{1}^{0/+}$ and $\mathbf{1}^{*/+}$ (omitted for clarity) are 0.75 and −1.10 V, respectively. All values are referenced to the oxidation of ferrocene (−4.8 V vs vacuum).

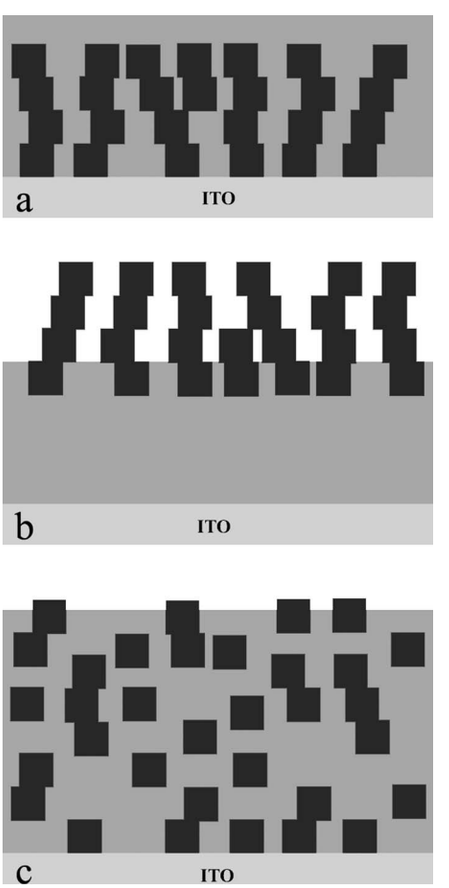

Figure 5. Schematic representation of the layer-by-layer growth geometries. (a) Interdigitated film: Layers of porphyrin compounds **1** or **2** (dark squares) are permeable to subsequently grown **3**. (b) Bilayer film: Layers of perylene-diimide **3** are not permeable to subsequently grown **2**. (c) Composition-randomized film: Porphyrin **1** or **2** and the perylene **3** are codeposited from the solution and thus grow randomly.

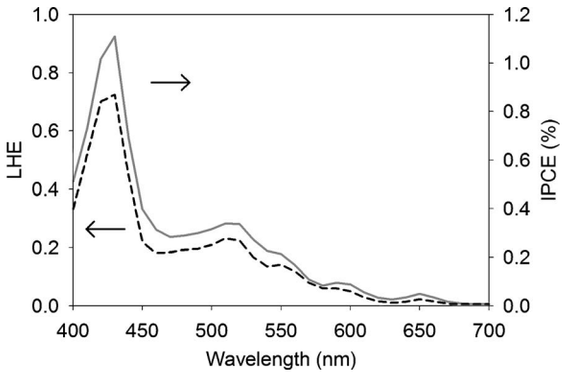

Figure 6. LHE (dashed line) and short-circuit photocurrent action spectra (solid line) of a cell composed of 8 layers of **2** and 10 layers of **3**.

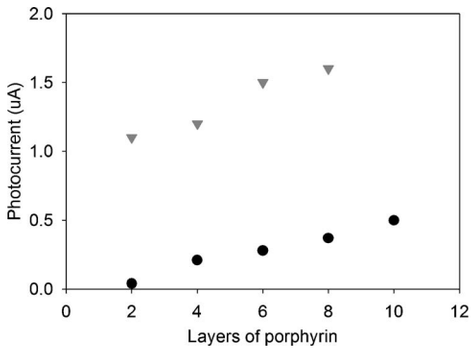

Figure 7. J_{SC} at the maximum absorbance as a function of the number of layers of **1** (circle) and **2** (triangle) in interdigitated donor/acceptor thin-film photocells. Multilayers of **1** and **2** are interdigitated with 20 and 10 layers of **3**, respectively.

the footprint of **3** is smaller than **2**, interdigitation should be absent and an electrode-supported bilayer structure (ITO/**3**/**2**) should form instead. Quenching was less efficient for this structure. In the third case, which we will designate **c**, **2**, and **3** were grown from the same solution to give a randomized structure. Photoluminescence quenching here was nearly quantitative.

The results of the electrochemical and fluorescence measurements are consistent with the formation of the desired interdigitated and preferentially oriented film structures. Furthermore, the observed quenching behavior indicates that the new structures are capable of functioning as fairly efficient heterojunctions. This result is not unexpected: in contrast to many blending schemes where the donor and acceptor are cocast or codeposited, the layer-by-layer growth and back-filling of porous frameworks should ensure high contact areas, negligible exciton transport distances, and nearly complete phase continuity. Indeed, as both porphyrin frameworks have previously been shown to be pinhole-free down to ~13 Å,[11,16] the scale of interdigitation must be similar.

The persistence of a modest amount of porphyrin luminescence, despite the interdigitated film design, could be indicative of sluggish excited-state electron-transfer dynamics. Alternatively, it could indicate that certain regions of the networked porphyrin film are inaccessible to the perylenediimide. That the second explanation is at least partially applicable is evidenced by the observation of more complete quenching in randomly assembled (type **b**) films. Perylenediimide inaccessibility might be caused by blockage of porphyrin film interstices by zirconium dioxide species. Both Librera et al. and Doron-Mor et al. have found excess zirconium in layer-by-layer assembled Zr-phosphonate films.[19,20]

Photocell behavior.— For a completed cell with 8 layers of **2** interdigitated and coated with 10 layers of **3** and an evaporated Al anode, the maximum IPCE at short circuit conditions is ~1% (Fig. 6). Typical open-circuit voltages (V_{OC}) under white light illumination for cells incorporating at least 4 layers of either **1** or **2** are greater than 300 mV. As expected, cells constructed with more layers show larger short-circuit currents (J_{SC}) at their respective absorbance maxima (Fig. 7). In relatively thick devices in which more than 20 layers of **2** and **3** are interdigitated the trend breaks down and device performance dramatically drops. For comparison, we also fabricated devices with traditional bilayer (type **B**) and codeposited (type **C**) heterojunctions that exhibit similar LHE to the interdigitated structure. The IPCE values for devices utilizing these traditional cell architectures are more than an order of magnitude lower and the V_{oc} values are less than 1 mV.

We initially envisioned photovoltaic behavior based on a sequence of light absorption by the porphyrin component followed by electron transfer from the photoexcited porphyrin to the perylenediimide component. The photocurrent action spectrum in Fig. 6, however, shows that productive light absorption also occurs with the perylenediimide. Notably, transport occurs in the same direction as with porphyrin excitation: holes migrate through the porphyrin framework to the ITO, while electrons traverse the perylenediimide layers to be collected at the aluminum anode.

One energetically feasible sequence to account for the additional sensitization is reductive quenching of photoexcited perylenediimide by porphyrin

$$\mathbf{2} + \mathbf{3}^{\star} \rightarrow \mathbf{2}^{+} + \mathbf{3}^{-} \qquad [1]$$

Another is energy transfer from photoexcited perylenediimide to porphyrin, followed by the already established oxidative quenching of photoexcited porphyrin by ground-state perylenediimide

$$\mathbf{2} + \mathbf{3}^{\star} \rightarrow \mathbf{2}^{\star} + \mathbf{3} \rightarrow \mathbf{2}^{+} + \mathbf{3}^{-} \qquad [2]$$

The sequence in Eq. 2 should lead to emission from the porphyrin when the perylenediimide is irradiated, because quenching will be incomplete. Equation 1 will not sensitize porphyrin luminescence. We find no significant porphyrin luminescence when the perylene is selectively excited, implying Eq. 2 is not a major contributor to the additional photocurrent generation.

Turning to cell efficiencies, devices featuring the interdigitated architecture exhibited J_{SC} and V_{OC} values superior to those obtained for a bilayer design. In view of the differences in photoluminescence for these two types of devices, part of the observed difference in energy conversion efficiency can be ascribed to differences in interfacial area. Another factor may be architecture-dependent effects of the internal field, i.e., the field arising from the difference in work function for ITO vs aluminum. For the interdigitated cell, the field should assist charge separation. In the bilayer cell, however, charges move in directions opposed by the field: electrons move toward the ITO electrode and holes move toward the aluminum electrode.

The interdigitated devices also consistently outperform those featuring composition-randomized structures. Given the similar LHE yet inferior η_{ED} of the interdigitated devices, explanations other than exciton transport and splitting must be considered. We suggest that the result can be understood in terms of enhanced phase connectivity and vectoral charge transport leading to greater effective charge migration and, hence, better performance.

Despite the performance advantages relative to optically similar bilayer and composition-randomized cells, the absolute photocurrent output of the interdigitated cells is low. In the most efficient interdigitated devices examined, the product of the LHE and η_{ED} is approximately 50% at 420 nm. Because the IPCE is the product of these two factors and the η_{CC}, the majority of IPCE losses must result from a failure to collect the separated charges at the desired electrodes. The above studies of electrochemical communication between **3** and the ITO electrode highlight one aspect of the charge-collection problem. Because **3** spans the thickness of the cell, the two electrodes can communicate via the electron acceptor columns

and electrons can be delivered to the wrong electrode. Additionally, shunts of this kind have been shown to have deleterious effects on the open-circuit photovoltages in organic photovoltaics.[21] In principle, the layer-by-layer strategy for heterojunction assembly presents opportunities for circumventing this problem that are unexplored in this work. For example, electron-blocking species selectively grown on the functionalized ITO substrate after the donor framework is formed but before the electron acceptor is added should eliminate the shunting behavior.

A second factor, almost certainly, is poor carrier transport dynamics. In comparison to highly conjugated layer interconnects, the zirconium phosphonate linkages will slow charge hopping toward the respective electrodes, increasing the steady-state concentrations of both carriers, and presumably increasing recombination.

A third factor may be over-miniaturization of the interdigitating structures. While reducing these to the molecular scale does appear to solve the exciton migration problem, it may well be that somewhat larger structures, say, bundled molecular strands 10 or 20 nm in width rather than isolated strands of 1 or 2 nm width, would be equally effective in this regard. Bundled structures would reduce the number of encounters between holes and electrons, thereby reducing recombination. The ideal width would be one equaling, but not appreciably exceeding, the lateral exciton transport distance. The work of Yang et al. on back-filled arrays of organic crystalline columns of greater than molecular width may be an example of a system approaching this ideal configuration.[22]

Conclusion

Heterojunctions interdigitated on the molecular scale can be constructed via a layer-by-layer self-assembly strategy. These interdigitated heterojunctions exhibit fair (at best) light harvesting efficiency while providing ample exciton dissociation area and circumventing the issue of exciton diffusion. When a dark electrode is added, the assemblies function as molecular photovoltaics. While clearly outperforming optically similar bilayer and composition-randomized heterojunctions, devices based on the interdigitated heterojunction exhibit very low absolute incident-photon-to-current efficiencies. In the most efficient of these cells, the photocurrent is most likely limited by a large charge recombination area and by poor charge carrier migration dynamics.

Acknowledgments

J.T.H. gratefully acknowledges support from the Basic Energy Sciences Program, Office of Science, U.S. Department of Energy under grant no. DE-FG02-87ER13808. S.T.N. acknowledges support from the Institute for Environmental Catalysis at Northwestern. A.B.F.M. and A.M.M. thank the Link Foundation for support as graduate fellows. R.W.G. acknowledges postdoctoral fellowship support from the Camille and Henry Dreyfus Foundation.

Northwestern University assisted in meeting the publication costs of this article.

References

1. G. Yu and A. J. Heeger, *J. Appl. Phys.*, **78**, 4510 (1995).
2. F. Padinger, R. S. Rittberger, and N. S. Sariciftci, *Adv. Funct. Mater.*, **13**, 85 (2003).
3. J. J. M. Halls, C. A. Walsh, N. C. Greenham, E. A. Marseglia, R. H. Friend, S. C. Moratti, and A. B. Holmes, *Nature (London)*, **376**, 498 (1995).
4. A. Haugeneder, M. Neges, C. Kallinger, W. Spirkl, U. Lemmer, J. Feldmann, U. Scherf, E. Harth, A. Gugel, and K. Mullen, *Phys. Rev. B*, **59**, 15346 (1999).
5. P. Peumans, A. Yakimov, and S. R. Forrest, *J. Appl. Phys.*, **93**, 3693 (2003).
6. L. Schmidt-Mende, A. Fechtenkotter, K. Mullen, E. Moons, R. H. Friend, and J. D. MacKenzie, *Science*, **293**, 1119 (2001).
7. T. J. Savenije, J. E. Kroeze, M. M. Wienk, J. M. Kroon, and J. M. Warman, *Phys. Rev. B*, **69**, 155205 (2004).
8. T. Hasobe, H. Imahori, S. Fukuzumi, and P. V. Kamat, *J. Phys. Chem. B*, **107**, 12105 (2003).
9. A. B. Pangborn, M. A. Giardello, R. H. Grubbs, R. K. Rosen, and F. J. Timmers, *Organometallics*, **15**, 1518 (1996).
10. K. E. Splan, A. M. Massari, and J. T. Hupp, *J. Phys. Chem. B*, **108**, 4111 (2004).
11. K. E. Splan and J. T. Hupp, *Langmuir*, **20**, 10560 (2004).
12. J. T. Kern and S. M. Kerwin, *Bioorg. Med. Chem. Lett.*, **12**, 3395 (2002).
13. A. M. Massari, R. W. Gurney, C. H. K. Huang, M. D. Wightman, S. T. Nguyen, and J. T. Hupp, *Polyhedron*, **22**, 3065 (2003).
14. G. Cao, H. G. Hong, and T. E. Mallouk, *Acc. Chem. Res.*, **25**, 420 (1992).
15. J. L. Snover, H. Byrd, E. P. Suponeva, E. Vicenzi, and M. E. Thompson, *Chem. Mater.*, **8**, 1490 (1996).
16. A. M. Massari, R. W. Gurney, C. P. Schwartz, S. T. Nguyen, and J. T. Hupp, *Langmuir*, **20**, 4422 (2004).
17. S. B. Ungashe, W. L. Wilson, H. E. Katz, G. R. Scheller, and T. M. Putvinski, *J. Am. Chem. Soc.*, **114**, 8717 (1992).
18. H. E. Katz, *Chem. Mater.*, **6**, 2227 (1994).
19. J. A. Libera, R. W. Gurney, S. T. Nguyen, J. T. Hupp, C. Liu, R. Conley, and M. J. Bedzyk, *Langmuir*, **20**, 8022 (2004).
20. I. Doron-Mor, H. Cohen, S. R. Cohen, R. Popovitz-Biro, A. Shanzer, A. Vaskevich, and R. I., *Langmuir*, **20**, 10727 (2004).
21. H. J. Snaith, N. C. Greenham, and R. H. Friend, *Adv. Mater. (Weinheim, Ger.)*, **16**, 1640 (2004).
22. F. Yang, M. Shtein, and S. R. Forrest, *Nat. Mater.*, **4**, 37 (2005).